The Astrophysical Journal, 970:117 (11pp), 2024 August 1 https://doi.org/10.3847/1538-4357/ad4c67

Experimental Vapor Pressure Determination for C_2H_4, C_2H_6, CH_3OH, CH_4, CO, CO_2, H_2O, and N_2 Molecules for Astrophysical Relevant Temperatures. Implications for the Presence of Volatiles in Kuiper Belt Objects and Trans-Neptunian Objects

C. Millán[1,2], R. Luna[1,2], M. Domingo[1,2], C. Santonja[1,2], and M. Á. Satorre[1,2]
[1] Departamento de Física Aplicada, Universitat Politècnica de València, Plaza Ferrándiz-Carbonell, E-03801 Alcoy Spain; cmillan@fis.upv.es
[2] Centro de Tecnologías Físicas, Universitat Politécnica de Valéncia, Plaza Ferrándiz-Carbonell, E-03801 Alcoy, Spain
Received 2023 July 28; revised 2024 May 7; accepted 2024 May 11; published 2024 July 24

Abstract

Vapor pressure is a relevant quantity that is necessary in order to improve the study of the atmosphere dynamics that take place within astrophysical scenarios. The aim of this study was to obtain the vapor pressure values of the following molecules: C_2H_4, C_2H_6, CH_3OH, CH_4, CO, CO_2, H_2O, and N_2 through experimentation, as well as to determine their empirical relationship with the temperature, applying the results to the persistence of volatiles in trans-Neptunian objects (TNOs) and Kuiper Belt objects (KBOs). The experimental determination was performed by measuring the sublimation rate for each molecule at different temperatures. The Hertz–Knudsen equation was used to obtain the vapor pressures for the aforementioned molecules, taking the necessary considerations into account, and the sublimation rate was measured using a quartz crystal microbalance. In order to check the validity of the methods used, the results obtained for water ice were compared with those of previous studies from the literature. The values obtained for CO, N_2, and CH_4 are of particular interest in the study of the TNOs' and KBOs' atmosphere composition. The results of this study improve the understanding of the surface and atmospheric composition of objects in the cold scenarios of the solar system, in particular, in KBOs and TNOs.

Unified Astronomy Thesaurus concepts: Experimental techniques (2078); Planetary atmospheres (1244); Surface ices (2117)

1. Introduction

Ices are present in a large variety of astrophysical scenarios. With regard to the solar system, a complete compilation of their presence on icy satellite surfaces can be found in Dalton et al. (2010). Likewise, the presence of molecules in their solid state in comets and interstellar medium has also been reported. In addition, the Cosmic Ice Laboratory at NASA's Goddard Space Flight Center has compiled an extensive list of detections.[3]

The sublimation and condensation of ices play a very important role in the formation, physical behavior, and composition of surfaces and atmospheres in the solar system. For example, in areas illuminated by the Sun on Pluto and Triton, N_2 ice sublimes and becomes part of the atmosphere, enabling it to flow and redeposit onto colder surfaces. As a result, the atmosphere of both of these solar system objects is regulated by the sublimation and deposition rates (Fray & Schmitt 2009).

The study of the sublimation of these molecules is considered particularly relevant in Kuiper Belt objects' (KBOs) environment. Schaller & Brown (2007) and Brown et al. (2011) studied the escape of volatiles in some KBOs, with the aim of explaining the diversity of the surface volatiles content, as well as the absence of volatiles at these bodies. The aforementioned studies focused on applying the Jeans escape model are based on the assumption that it is the slowest of all mechanisms used to explain the escaping of volatiles at low columnar densities. This therefore means that it could be considered as an upper limit for how long a molecule remains on a particular astronomical object. As can be seen in the text, new escape mechanisms depending on the atmosphere molecules concentration can be even slower. We applied the hydrodynamic mechanism to the case of N_2 molecule.

In our study it appears molecules such as CH_4, N_2, and CO are of great interest because their presence has already been confirmed in previous studies: CH_4 on the surface of Makemake (Licandro et al. 2006 and Perna et al. 2017); CH_4 and N_2 in Eris (Tegler et al. 2010); solid CO, N_2, and CH_4 in Pluto (Owen et al. 1993) and Triton (Cruikshank et al. 1993; Grundy et al. 2016); and in Quaoar, CH_4, CO_2, and N_2 from the shift of the CH_4 bands, and CO molecules diluted in N_2 has been suggested (Barucci et al. 2015). In addition, the presence of N_2 and CH_4 in Sedna's surface composition is possible (Barucci et al. 2005).

Subsequent studies have included other mechanisms that would complement the Jeans escape mechanism; the phenomenon on which the works of both Schaller & Brown (2007) and Brown et al. (2011) are based. According to Volkov et al. (2011a, 2011b), in the case of the most volatile molecule, that is to say, N_2, if the column density is higher than 10^{14} molecule·cm^{-2}, hydrodynamic molecule transport comes into play.

Likewise, in other cases in which the N_2 column density is greater than 10^{18} molecules cm^{-2}, the CH_4 concentration increases to the point in which the role of atmospheric heating on escaping seems to be gaining relevance (Johnson et al. 2013a, 2013b, 2015). Regardless of the dominant procedure that provokes the removal of the molecules from the atmosphere of an astronomical object, the column density depends on the vapor pressure, and this in turn depends on the temperature, therefore justifying the realization of this present study.

The database previously used in the literature for vapor pressure was obtained from the study by Lodders & Fegley (1998; hereinafter L-F), in which the temperatures used were

[3] https://science.gsfc.nasa.gov/691/cosmicice/

higher than those found in KBOs; specifically, 65–90.6 K for CH_4, 50–68.1 K for CO, and 54.78–63.14 K for N_2. As a result, in L-F they were obliged to apply an extrapolation of the corresponding values to the temperatures of interest, using a version of the Clausius–Clapeyron equation:

$$\log P_v = a + \frac{b}{T} \quad (1)$$

in which P_v is the vapor pressure and a and b are two fitting parameters provided in that book.

An extensive compilation study of the sublimation rates and vapor pressures of several ices of astrophysical interest can be found in Fray & Schmitt (2009; hereinafter F-S). Due to that, there are limited experimental data on temperatures between 20 and 50 K for CO and CH_4; these data are usually extrapolated using a specific equation, which is different for each molecule. The experimental temperature widely covered the interval of interest for N_2. The values offered by F-S continue to be used in works on stability in different objects (Lisse et al. 2021).

Together with these data sets, other experimental studies can be considered for specific molecules, as is the case of Bryson et al. (1974) for CO_2 and Lucas et al. (2005) for CH_3OH.

The vapor pressures that have been included in the present study for CO and CH_4 were obtained through experimentation and cover temperatures between 20 and 50 K. Together with the work of Grundy et al. (2024) this means that they better represent the values found on KBOs. In addition, data for C_2H_6 are also presented covering a temperature range of around 20 K above the temperatures found in the solar system context, but closer than the experimental data referred to in the study by F-S.

The presence of other ices, such as CO_2 (McCord et al. 2008; Coustenis et al. 2007), CH_3OH (Dalle Ore et al. 2015; Cook et al. 2019), C_2H_4 (Coustenis et al. 2007), and C_2H_6 (Barucci et al. 2015) are well known in the solar system; therefore, the vapor pressures for these ices were also measured in this study.

For this set of molecules, however, the temperature data range is restricted to those in which the sublimation rate was higher enough to be measured by means of quartz crystal microbalance (QCMB). These temperature intervals do not necessarily match with the temperatures that can be found in KBOs or trans-Neptunian objects (TNOs).

The reliability of the present study was guaranteed through the use of a QCMB. The QCMB is an accurate device that can be used to obtain sublimation rates for a species, and it directly detects molecules that are being released from the solid surface.

2. Experimental Setup

The experiments were conducted in a system working under high vacuum conditions. The main components were a QCMB, a double laser interferometer, which is used to measure the film thickness during growth, and a temperature controller (Figure 1). The base pressure during the experiment (3×10^{-7} mbar) was obtained by assembling a pair of turbo-molecular pumps that were supported by their corresponding rotary pumps and aided by a closed-cycle He cryostat acting as a cryopump. To obtain a constant flow of molecules entering the chamber during accretion, the two following parameters were regulated: the pressure in the prechamber, which was measured with a capacitive sensor, and the aperture of a needle valve at the entrance.

The edge of the cryostat was in thermal contact with the QCMB (Q-Sense gold-coated quartz, $f_0 = 5$ MHz). To improve the thermal conductivity, our QCMB is mounted on a sample holder made of aluminum. Also, the sample holder and the cold finger were put into thermal contact through a thin layer of indium. The QCMB and the temperature sensor were fixed with copper strips attached to the sample holder with screws. The temperature of the sample that was deposited onto the QCMB was regulated using an Intelligent Temperature Controller (ITC) 503S intelligent temperature controller (Oxford Instruments) with a silicon diode sensor (Scientific Instruments) located 5 mm below the quartz crystal and attached to the cold finger with the same copper strip. By using the ITC, it was possible to vary the temperature between 10 K and room temperature with 0.5 K accuracy.

The reliability of the experimental setup shown is certified according to the coherence of other measurements carried out at low temperatures, which will be mentioned below.

The QCMB component of the experimental system was used to measure the release rates from the surface of the volatiles under study. The QCMB makes use of the piezoelectric features of a quartz crystal and vibrates transversely with a frequency that is dependent on its physical characteristics, that is to say, its density, shear modulus, thickness, and temperature.

If a gas is accreted on the QCMB, the mass load causes a decrease in the frequency in relation to the mass deposited. The relationship between the mass deposited and the frequency decrease depends on the ratio between the mass load and the mass of the quartz film (Benes 1984), and this can be quite complex in some cases. However, for mass ratios $m_f/m_q < 2\%$ (where m_f and m_q represent the mass load and mass of the QCMB, respectively) the linear relationship proposed by Sauerbrey (1957, 1959) can be applied:

$$\Delta f = -S \cdot m_f \quad (2)$$

where S is the Sauerbrey constant, and for reasons of accuracy, this constant must be determined for every experimental assembly. In this study, the value can be found in Luna et al. (2012).

3. Experimental Procedure

The experiment that was conducted to obtain a single value for vapor pressure at a certain temperature consisted of an initial mass deposition at a constant rate and a further desorption at a constant temperature. When the sample holder reached a temperature of 14 K, the gas was introduced into the chamber, and it froze onto the cold substrate. This accretion resulted from the atmosphere created in the chamber, without any preferential directions, a process referred to as a background deposition. By keeping constant pressure inside the chamber, it was possible to achieve a constant deposition rate.

The thickness of the film was controlled by means of the interference pattern obtained with the double laser interferometric system He−Ne (632.8 nm). Figure 2 shows the frequency decrease recorded when CO is deposited at 14 K. When a thickness of approximately 1.9 μm was achieved, the deposition was stopped. For this molecule, this thickness corresponds with a mass of 0.17 mg (Luna et al. 2022). As can be observed in Figure 2, the film growth was carried out for around 1400 s, which means that the deposition rate was around 0.12 $\mu g\ s^{-1}$. Under these conditions, the linearity of the curve plotting frequency versus deposited mass at constant temperature, represented by Equation (2), is fulfilled.

It is important to note that, after closing the high vacuum chamber inlet valve, the QCMB signal remains constant, which

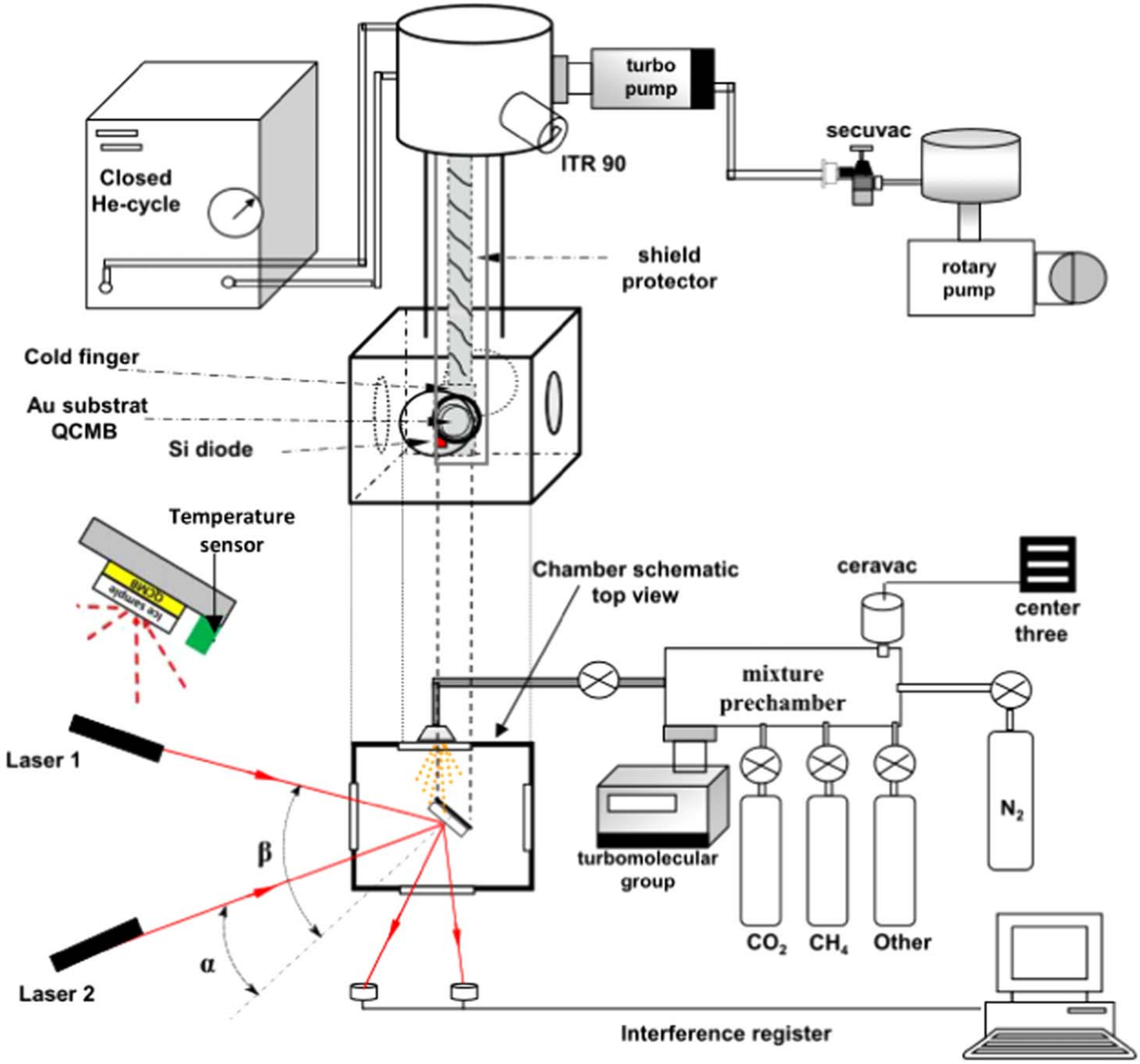

Figure 1. The main components of the experimental setup are indicated, showing the positioning of the laser beams and the locations of the QCMB, the sample, and one of the temperature sensors.

indicates how efficiently our off-gassing system works for this molecule. For the rest of the molecules, the mass rate deposition, the thickness, deposited mass, deposition mass rate, as well as the behavior after to stop the deposition were similar.

After deposition, the temperature of the sample holder was raised at a constant rate until it reached a set of temperatures that were below the sublimation peak (the temperature at which the sublimation rate is maximum under our experimental conditions). These temperatures were taken from Luna et al. (2018).

In this experiment, the sublimation rate ($r_{\rm sub}$) for each species was determined using the following expression:

$$r_{\rm sub} = \frac{1}{S} \cdot \frac{\Delta f}{\Delta t} \cdot \frac{1}{M} \cdot N_A \tag{3}$$

where S is the aforementioned Sauerbrey constant for our QCMB, the quotient $(\Delta f/\Delta t)$ is the slope of the straight line obtained from the corresponding sublimation experiment at a constant temperature (Figure 3), M is the molar mass of the deposited species, and N_A is the Avogadro number. The units corresponding to the sublimation rate are molecule$\cdot\,{\rm s}^{-1}\,{\rm cm}^{-2}$.

In Figure 3, the sublimation part for the experiment at $T = 30$ K is shown between the two vertical dashed lines for the case of CO. In order to keep a constant mass-loss rate, it is crucial to maintain a constant temperature during desorption.

The temperatures considered in these experiments ensured that the sublimation process represented a sufficient releasing molecules rate; therefore, meaning that it would be detectable from the QCMB signal under our experimental conditions.

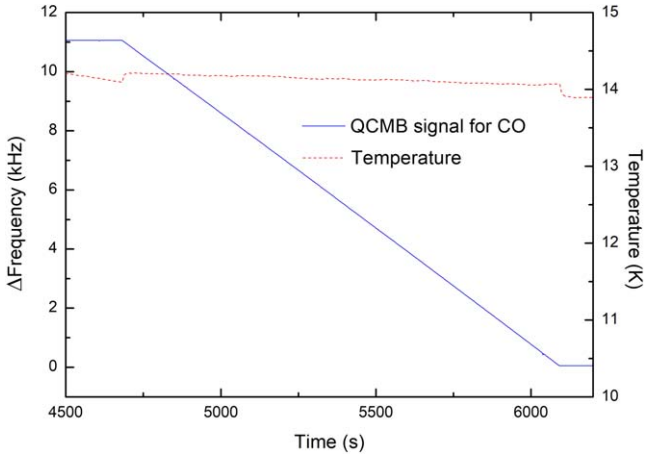

Figure 2. The QCMB signal (blue line) during deposition at a constant rate and temperature. The red dotted line corresponds to the temperature record.

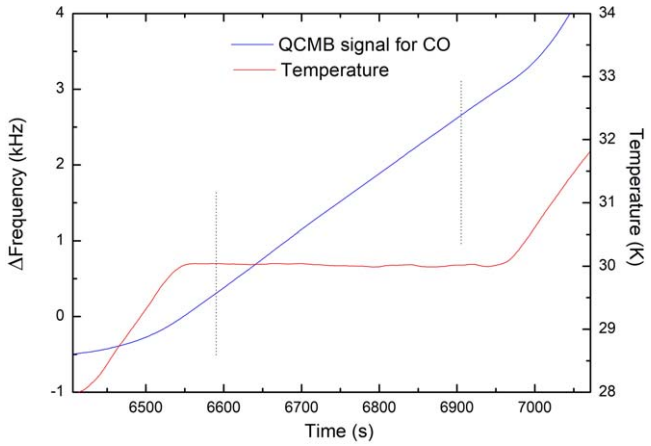

Figure 3. Desorption experiment at a constant temperature for CO to derive the vapor pressure at 30 K.

4. Theoretical Expression to Obtain the Vapor Pressure

On the one hand, in order to derive the vapor pressure from the sublimation rate, the molecules that have passed into the gas phase could return to the solid surface and eventually be trapped. The sublimation coefficient is defined as the quotient between the actual mass desorbed and the theoretical one. Therefore, this must be taken into account in order to prevent the underestimation of the vapor pressure.

On the other hand, and for a gas contained in a volume limited by walls, according to kinetic theory, the relationship between the pressure and the number of molecules that hit the unit of area per second from the gas state can be obtained using the Hertz–Knudsen equation:

$$\frac{dn}{A \cdot dt} = \frac{P \cdot N_A}{\sqrt{2 \cdot \pi \cdot M \cdot R \cdot T}} \tag{4}$$

in which P *(Pa)* is the gas pressure on the surface, N_A is the Avogadro number, M is the molar mass (kg), R is the gas constant (J mol^{-1} K^{-1}), and T is the absolute temperature of the gas phase on the right side of the equation. On the left side of the equation, n is the number of molecules and A (m^2) is the area of the surface onto which the molecules fall.

Molecules hitting a cold surface may or may not be trapped, and, as such, a parameter α is introduced in Equation (4), taking into account the molecule ratio for trapped molecules. Therefore, the following equation can be used to calculate the molecules that are trapped after hitting a cold surface.

$$\frac{dn}{A \cdot dt} = \frac{\alpha \cdot P \cdot N_A}{\sqrt{2 \cdot \pi \cdot M \cdot R \cdot T}}. \tag{5}$$

Likewise, an ice sample can be considered as a recipient that contains a gas with a pressure P_v (the vapor pressure). In this case, the molecules would be considered as if they were in the gaseous phase inside the sample, hitting the sample boundaries and either getting out or bouncing back. As a result, by introducing the suitable parameters, it is also possible to use Equation (5) to obtain the sublimation rate of an ice sample at T_s (sublimation temperature).

$$\left(\frac{dn}{A \cdot dt}\right)_{\text{sub}} = \frac{\alpha_v \cdot P_v \cdot N_A}{\sqrt{2 \cdot \pi \cdot M \cdot R \cdot T_s}} \tag{6}$$

where P_V is the vapor pressure (saturation pressure) and α_v is a parameter that considers the possibility for the molecules to return to the sample after they have been released, similar to α in Equation (5), but in this case, the molecules are inside the sample, because we are regarding imaginary walls to contain the gas. In fact, in Langmuir (1913), this equation appears without the coefficient.

The number of molecules released from a cold sample is obtained by subtracting Equation (5) from Equation (6).

$$\begin{aligned}\left(\frac{dn}{A \cdot dt}\right)_{\text{rel}} &= \frac{\alpha_v \cdot P_v \cdot N_A}{\sqrt{2 \cdot \pi \cdot M \cdot R \cdot T_s}} - \frac{\alpha \cdot P \cdot N_A}{\sqrt{2 \cdot \pi \cdot M \cdot R \cdot T}} \\ &= \left(\frac{\alpha_v \cdot P_v}{\sqrt{T_s}} - \frac{\alpha \cdot P}{\sqrt{T}}\right) \cdot \frac{N_A}{\sqrt{2 \cdot \pi \cdot M \cdot R}}.\end{aligned} \tag{7}$$

The pressure and the temperature of the gas phase over the sample is represented by P and T, respectively. The temperature T in Equation (7) could be considered equal to T_r, T room, given that the majority of the molecules would hit the walls of the chamber before the QCMB. The units in all these equations (Equations (4)–(7) are molecule$\cdot$ s^{-1} cm^{-2}.

If we disregard the second term in Equation (7) and assume a value of $\alpha_v = 1$ (for the same reason, α can be considered equal to 1) at the sublimation temperature range for all the molecules included in this study, leading us to determine that:

$$\left(\frac{dn}{A \cdot dt}\right)_{\text{sub}} = \left(\frac{dn}{A \cdot dt}\right)_{\text{rel}} = \frac{P_v \cdot N_A}{\sqrt{2 \cdot \pi \cdot M \cdot R \cdot T_s}}. \tag{8}$$

Finally, the vapor pressure, that is to say, the pressure of the saturated vapor, can be obtained from

$$P_v = \frac{\sqrt{2 \cdot \pi \cdot M \cdot R \cdot T_s}}{N_A} \cdot \left(\frac{dn}{A \cdot dt}\right)_{\text{rel}}. \tag{9}$$

The term between parentheses on the right in Equation (9) would correspond to the experimental parameter measured in our laboratory.

The vapor pressure obtained from Equation (9) for H_2O, CO_2, and CH_3OH molecules in this study and the results

reported in previous studies are comparable. That said, allow us to conclude that the simplifications made are plausible.

Another argument in favor of neglecting the contribution of the influence of the molecules coming from different directions and sticking to the QCMB is the following: in Grundy et al. (2024) the parameter $\varphi = \frac{P_{\mathrm{QCMB}}}{P_{\mathrm{gauge}}}$ has been calculated, in which P_{QCMB} and P_{gauge} represent the pressures on the QCMB and that measured by their pressure gauge.

It is obvious that this parameter takes a value depending on the specific experimental setup, but it can be considered as an approach. In the present research, for the case of the N_2, a vapor pressure of 1.5×10^{-3} Pa was obtained at 27 K.

During the experiments, a mass spectrometer recorded the pressure in the chamber. Along the sublimation at 27 K, the mass spectrometer recorded a maximum pressure of 9.5×10^{-5} Pa (P_{gauge}). From the plot obtained in Grundy et al. (2024) for this temperature, a pressure of 8.2×10^{-5} Pa would correspond approximately with that actually experienced by the QCMB surface in our experimental setup.

In Equation (7), the contributions of the addends in parentheses are 3×10^{-4} (for pressure vapor of 1.5×10^{-3}, as noted above) and 4.7×10^{-6} Pa $K^{-0.5}$ (we should not lose sight, for the reasons expressed above, that α and α_v are considered equal to 1), the first for the contribution of vapor pressure, and the second for the pressure due to the molecules that travel free throughout the chamber. The first term is 2 orders of magnitude larger than the second, i.e., the molecules that return to the QCMB are lesser than 2% with respect to the released. This led us to neglect the contribution of the second addend within the parenthesis in Equation (7).

5. Vapor Pressures for H_2O, CO_2, CO, CH_4, CH_3OH, C_2H_6, C_2H_4, and N_2

5.1. Water

With regard to water vapor pressure, a considerable amount of experimental and theoretical data and empirical expressions are available. In this study, this molecule was selected to check the validity of the method used. The works of Murphy & Koop (2005), F-S, Mauersberger & Krankowsky (2003), and Bryson et al. (1974) have been plotted in Figure 4 together with the results derived from Equation (9).

Murphy & Koop (2005) and F-S obtained the vapor pressure in a similar way. The Clausius–Clapeyron equation was applied, considering a latent heat dependent on the temperature. Experimental values of latent heat were used at the triple point of water, and heat capacities were used at constant pressure. However, the equation used to obtain a functional relationship was not completely identical. In Bryson et al. (1974), we have taken into account the experimental values reported. In Mauersberger & Krankowsky (2003), the linear fit obtained from the experimental results was considered.

The values obtained in this work, and shown in Figure 4, were consistent with the previously reported expressions at and below 172 K. Above this temperature, a small discrepancy is detected that, in addition, does not vary with temperature. This could also be detected for CO, CO_2, H_2O, N_2, and C_2H_6 at the highest temperature. This means that it is possible to infer a value of 1 for α coefficient for temperatures below 175 K and to discard the second term to the right part of Equation (7).

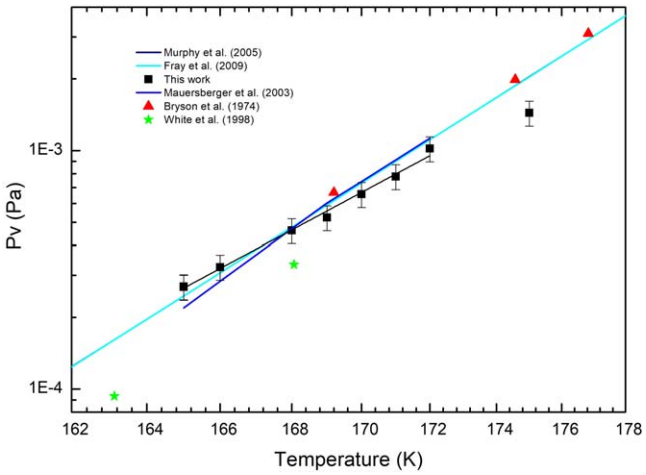

Figure 4. Comparison between the water vapor pressures obtained in this study and the values calculated from the empirical equations obtained by Murphy & Koop (2005) Fray & Schmitt (2009), neatly superimposed, Mauersberger & Krankowsky (2003), and the experimental values obtained by Bryson et al. (1974) and White et al. (1998).

Table 1
Parameters for the Linear Fit Performed, R^2, and Selected Temperature Range

Molecule and Purity (%)	a	$b \cdot 10^{-3}$ (K)	R^2	Temperature Range (K)
Ethylene 99.95	10.7 ± 0.3	-0.95 ± 0.02	0.998	62–69
Ethane 99.99	14 ± 1	-1.23 ± 0.08	0.98	68–74
Carbon dioxide 99.998	12.6 ± 0.4	-1.44 ± 0.04	0.99	85–92
Methanol 99.9	11.1 ± 0.5	-2.12 ± 0.07	0.99	142–152
Water (triply distilled)	10.0 ± 0.4	-2.25 ± 0.05	0.99	165–175
Nitrogen 99.99	3.6 ± 0.3	-0.170 ± 0.007	0.99	21–27
Carbon monoxide 99.99	5.4 ± 0.2	-0.267 ± 0.006	0.99	24–32
Methane 99.99	8.9 ± 0.2	-0.467 ± 0.006	0.99	35–38

Note. The parameters a and b correspond to the parameters present in an equation using the log $P_v = a + b/T$ form.

5.2. CH_3OH, C_2H_4, CH_4, CO, CO_2, N_2, and C_2H_6

The experimental study was extended to CH_3OH, C_2H_4, CH_4, CO, CO_2, N_2, and C_2H_6 molecules. CH_3OH was obtained from Panreac UHPLC and the rest of the gases were from Nippon gases. The purity and the sources of the gases can also be found in Table 1.

Their vapor pressures were obtained through desorption experiments in a range of temperatures that were like those found in some astrophysical scenarios. Figure 5 shows the vapor pressures that were derived from the experiments conducted for all the molecules considered in this study. To assign error bars, the experiments were repeated up to five times for selected temperatures to check what the repeatability was. From these five values for the vapor pressure, we took the average value for each molecule and temperature, considering the uncertainty of this estimation as the semiamplitude of the 95% confidence interval (Student's t-distribution). As a consequence, for all the experiments the relative error that can be assigned to each value was about 12%.

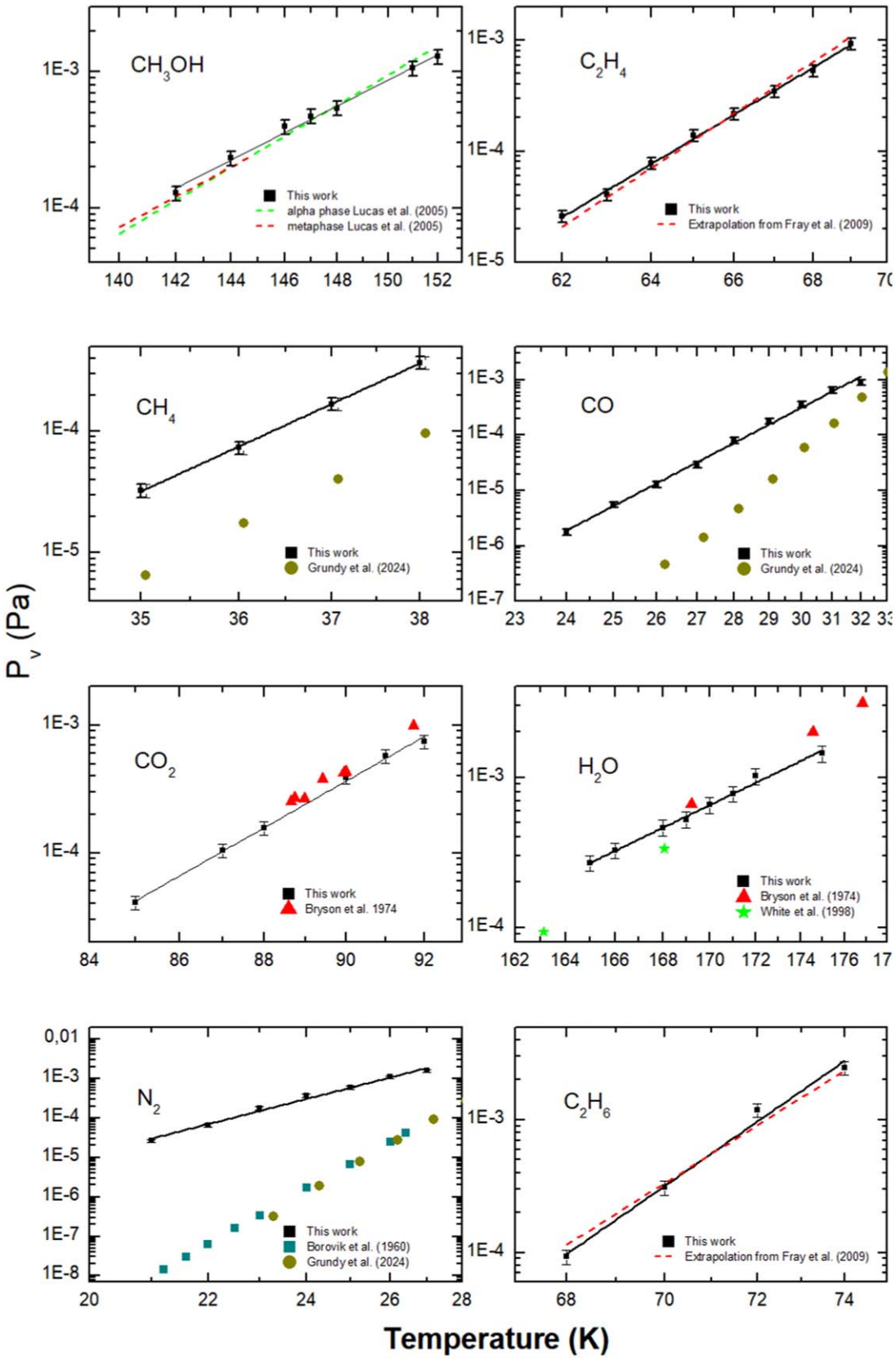

Figure 5. Experimental vapor pressure vs. temperature for the molecules under study. Black points with error bars and black solid lines are the results of this work and corresponding linear fits. Not connected points are experimental points from other works. For C_2H_4 and C_2H_6, red dashed lines are obtained from equations in Fray & Schmitt (2009) for temperature ranges without experimental data available. For CH_3OH, green and red dashed lines correspond to extrapolation for alpha and metastable phases, respectively, obtained in Lucas et al. (2005). For N_2, CO, and CH_4 see Figure 5 for a wider set of experimental and nonexperimental data sets.

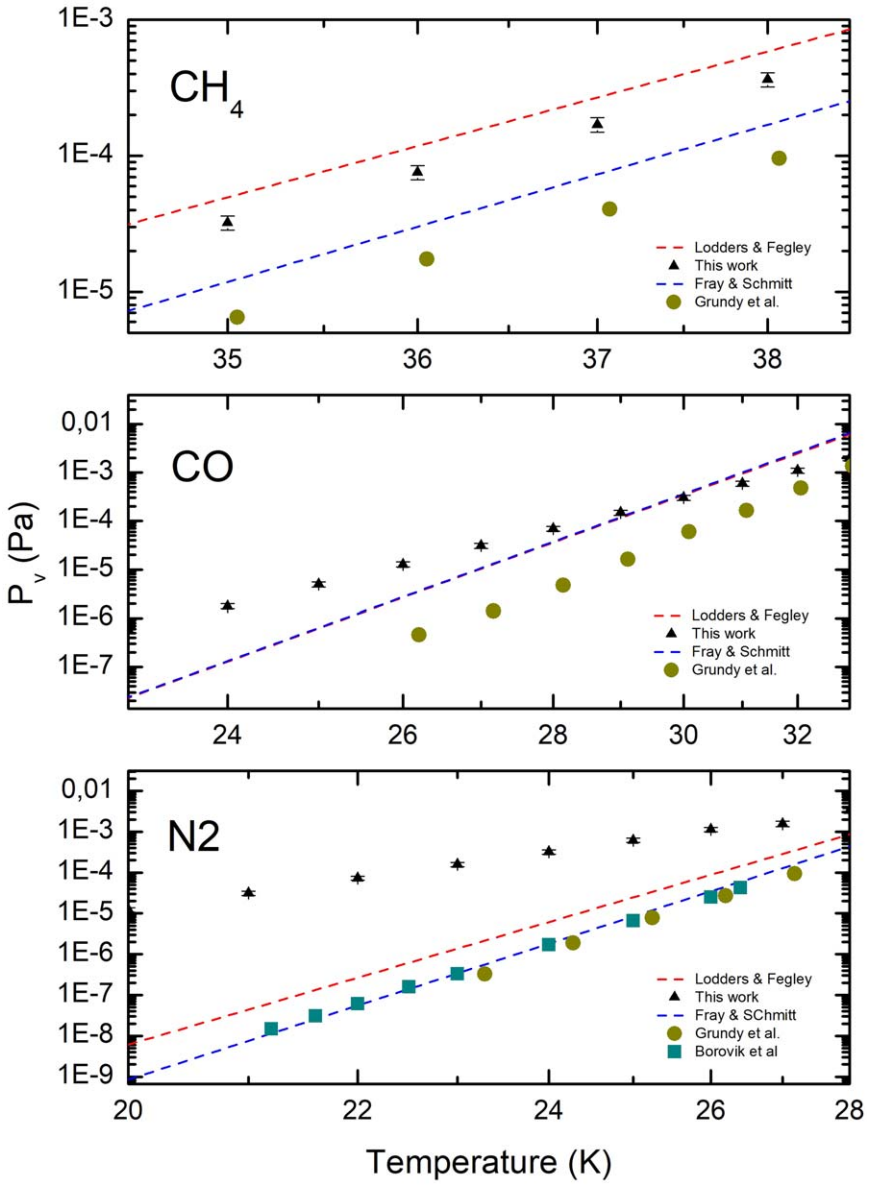

Figure 6. Comparison of the vapor pressures for N_2, CO, and CH_4 from the works of L-F, F-S, and Grundy et al. (2024) with those obtained in this present study. Also, data from Borovik et al. (1960) for N_2 have been included.

Additionally, in order to facilitate the calculation of vapor pressures for the corresponding range of temperatures for each molecule, in Table 1 the parameters a and b together with the value of the coefficient R^2 (which represents the goodness of the fitting), and the range of the experimental temperatures for each molecule for a linear fitting similar to Equation (1) is reported.

All the values obtained for R^2 were higher than 0.98, which therefore meant that it was possible to derive a reliable expression to relate P_V to T for the range of temperatures under study for each molecule.

6. Application to Volatiles on Cold Bodies in the Solar System

Vapor pressure is a relevant quantity that is used to calculate the escape of molecules from KBOs and TNOs, and this, in turn, has an important weight on the composition of both ices and atmospheres of these solar system objects. In Figure 6, the vapor pressures for CO, CH_4, and N_2 obtained in our laboratory have been compared with the previous results reported by L-F and F-S, which needed to have been extrapolated to the range considered in this study, together with the very recent reported by Grundy et al. (2024).

For the case of CH_4, the values obtained in this study were between those attained by F-S and L-F, and above the Grundy et al. (2024) reports. For the CO molecule and up to 28 K, our values are higher than the F-S and L-F ones up to 29 K, and lower from 29 to 32 K. For the whole range of temperatures, our values are higher than those by Grundy et al. (2024). N_2 was the most remarkable, given that in this present study it acquired higher values than in the other data sets.

It is worth noting that one of the aims of this study was to compare the experimental data obtained with the extrapolations in the other data sets for CO and CH_4 molecules. Only in the case of Grundy et al. (2024), the data shown are obtained from experiments at the corresponding temperatures.

Also, it is interesting to note that, in those cases, the slopes of the linear fits are somewhat different, suggesting slightly different activation energies of the sublimation among studies.

The discrepancy between our results and previous ones is obvious. The experimental setup through which these measures were obtained has been checked several previous times. For instance, in Schulze & Abe (1980) the refractive index and density for CO_2 is obtained from temperatures below 10 K. In this work, if we look at the density shown at 20 K, the displayed value is between 1.0 and 1.1 $g\,cm^{-3}$. At 30 K, it is close to 1.2 $g \cdot cm^{-3}$. Our most recent measures for density at these temperatures were performed with the same experimental arrangement with which we have carried out the present study (Satorre et al. 2018) and, it can be observed that for these two temperatures, densities match quite well. Also, in Schulze & Abe (1980), density values presented a plateau between 10 and 15 K, reproduced in our experiments.

Although the behavior is more stable between 20 and 30 K in the case of CO, in Luna et al. (2022) and González et al. (2022) it is possible to check that the results of the density obtained from two different laboratories, the one where the present results have been obtained, and the Interstellar Astrochemistry Chamber, described in Muñoz Caro et al. (2010), also agree.

In this context, it is worth bringing up the detection of the metastable phase for ethylene between 22 and 35 K reported in Satorre et al. (2017) with the current experimental setup, as reported previously in Hudson et al. (2014).

In order to demonstrate how the results of this study could influence the prediction of the presence of these three molecules on the surfaces and atmospheres of some cold KBOs, the values of vapor pressure present in this study were used to update the similar curve that appears in Schaller & Brown (2007) and Brown et al. (2011). The result is shown in Figure 7. This plot represents the surface equivalent temperature and the object diameter for several cold objects. In order to calculate the equivalent temperature, the rate loss for N_2, CH_4, and CO at each position in the object's orbit was obtained, and this was integrated over the age of the solar system. Subsequently, the corresponding temperature of an identical object in a circular orbit that had lost the same mass over the age of the solar system was derived, as reported in the study by Schaller & Brown (2007).

Most of the KBOs lie within the left medium-upper zone of the graph (see Brown et al. 2011); however, these bodies were eluded in this plot given that they do not present the necessary conditions for the molecules to be in their solid form. In Figure 7, the solid lines represent the limits for the presence or absence of each of the volatiles studied in the case in which only the Jeans escape mechanism for the studied molecules is taken into account, considering only heating coming from the body surface. More precisely, this refers to the points of diameter and temperature for which the initial mass of each volatile has disappeared throughout its existence. The curves were determined by calculating the mass loss by means of the expressions used in Schaller & Brown (2007) and Brown et al. (2011) with our vapor pressure values.

To the left of each curve, the conditions for the bodies that are either too small or too hot to retain the corresponding molecule over the entire age of the solar system are given, and to the right of each curve, the objects that are still capable of retaining this volatile are given. The results differ from those previously published for the objects lying near the lines because small changes in the vapor pressure could imply the presence or absence of a certain species in the surface of a body.

In Brown et al. (2011) and our work, Makemake, Haumea, Sedna, Pluto, Triton, and Eris are well placed to the right of the curves. In Brown et al. (2011) Makemake is closer to the N_2 curve than in our work. Charon is placed to the left of the curves in the two works. The object 474640 Alicanto (2004 VN112) is found on the CH_4 curve in Brown et al. (2011); nonetheless, this does not affirm the idea that this molecule can be found on the surface of this body. In our study, this body is clearly found to the left of the graphs.

For the objects closer to the N_2, CO, and CH_4 curves in Brown et al. (2011), Quaoar and Gonggong (2007 OR 10), are placed over the CH_4 and to the left of the CO and N_2 lines. In our work Quaoar is placed on the right side of the CH_4 and CO curves and on the left of the N_2 one; and Gonggong (2007 OR 10) on the right side of the CO curve and on the left side of the CH_4 and N_2 ones, almost over the CH_4 curve.

For comparison reasons, the curves displayed for each molecule in Brown et al. (2011) have been plotted by using a data set from Fray & Schmitt (2009). As can be observed, for temperature ranges that appear in Figure 6, the three curves, according to our data, are shifted to the left in Figure 7. However, for N_2 and CO, because they have different slopes in Figure 6, we can assume that due to different activation energy, if a Clausius–Clapeyron form is admitted, there is a temperature in which our vapor pressure date set became smaller than the Fray & Schmitt (2009) one. This would explain why from a certain temperature, our curves in Figure 7 are located to the right of Brown et al. (2011). For the case of the CH_4 molecule, the vapor pressure in Figure 6 is almost parallel to the rest of the vapor pressures and with higher values than the Fray & Schmitt (2009) data set, which explains the slight shift to the right of the curve obtained with our values. At temperatures around 50 K, it seems that the two curves intersect. For the N_2 molecules, at the lower temperatures where differences between our data and Fray & Schmitt (2009) are very remarkable, the curve is offset to the right. For instance, at the temperature of 20 K, for Brown et al. (2011) the diameter limit takes the value of 200 km, whereas for us, around 500 km.

There is another physical mechanism that could modify the escape of volatiles from the bodies that appear in Figure 7, such as, for example, the retention of molecules inside a matrix of a more refractory ice with the highest sublimation temperature (Colling et al. 2004; Luna et al. 2008). According to a recent report published by Emery et al. (2024), there is a slight possibility of finding carbon monoxide in Quaoar. The chances that this happens are higher when getting our data than the previous one, according to the proximity and location of Quaoar with respect to the CO curve. Emphasizing that if the curve for CO is constructed using the data in Grundy et al. (2024), and if we disregard other mechanisms engaged in the escape process, it leans toward the right of Quaoar more remarkably, and that will mean the total absence of CO.

Subsequent works have drawn attention to the importance of other mechanisms that must be considered when assessing the volatile loss rate. The studies that have considered this subject (Volkov et al. 2011a, 2011b; Johnson et al. 2013a, 2013b, 2015) are focused on the ice of N_2, given that it is the most volatile species. According to these studies, if the column density of a species (N_0) is lower than 10^{14} molecule $\cdot\, cm^{-2}$, the sublimated molecules barely collide with each other, therefore meaning that

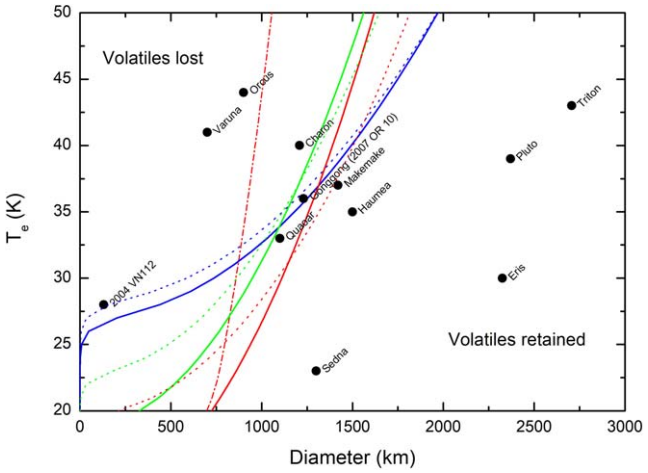

Figure 7. Objects to the left of a curve are not able to retain the corresponding volatile (methane in blue, nitrogen in red, and carbon monoxide in green), whereas the objects to the right are able, during the life of the solar system. The mechanism considered to obtain these curves is the Jeans escape (based only on the equilibrium surface temperature), and this represents the slowest procedure concerning the loss of volatiles at low columnar densities. Solid lines are our results, and dotted lines are Brown et al. (2011) for comparison purposes. The red dashed–dotted line curve corresponds to the values obtained, taking into account the corrections obtained by applying the hydrodynamic mechanism to our data.

the premises used by Schaller & Brown (2007) and Brown et al. (2011) are acceptable. However, if $N_0 \geqslant 10^{14}$ molecule$\cdot$ cm^{-2}, the assumptions made in the previous range are unrealistic. To this range, at the surface, the atmosphere becomes so dense that a hydrodynamic transport mechanism begins to gain importance. Both of these mechanisms are driven by surface heating. With this in mind, a modified curve was introduced for N_2 in Figure 7. This modification was made by applying the set of equations proposed in Johnson et al. (2015), Equations (10)–(15) below, in conjunction with the vapor pressures presented in this study. The following procedure was used, with the below equation as the starting point:

$$\left(\frac{dm}{dt}\right)_S \sim R_{\rm fit} \cdot \left(\frac{dm}{dt}\right)_{SJ}. \tag{10}$$

This Equation (10) was proposed in Johnson et al. (2015), and the mass lost for both mechanisms involved, $(dm/dt)_S$ and $(dm/dt)_{SJ}$, are related with a fitting parameter ($R_{\rm fit}$). The subscript *SJ* refers to the escape that is produced by the Jeans escape mechanism, and *S* refers to the escape that is produced when considering the hydrodynamic transport mechanism. $R_{\rm fit}$ is the parameter that allows for the correction of the values obtained from both models. Johnson et al. (2015) determined the following equation for this parameter:

$$\frac{1}{R_{\rm fit}} = (K_{n_0})^{0.09} + \frac{\lambda_0^{2.55}}{K_{n_0} \cdot e^{\lambda_0}} \tag{11}$$

where K_{no} refers to the radial Knudsen number, calculated from the Equation (12):

$$K_{n_0} = \frac{1}{\lambda_0 \sigma_{\rm eff} N_0} \tag{12}$$

in which λ_0 and $\sigma_{\rm eff}$ are the length of the mean free path (m) and the collisional cross (m^{-2}) section of N_2 molecules.

By introducing this expression in Equation (11), the following expression is obtained:

$$\frac{1}{R_{\rm fit}} = \left(\frac{1}{\lambda_0 \sigma_{\rm eff} N_0}\right)^{0.09} + \frac{\lambda_0^{2.55}}{\left(\frac{1}{\lambda_0 \sigma_{\rm eff} N_0}\right) \cdot e^{\lambda_0}}. \tag{13}$$

Previously, the values of the column density and the Jeans escape parameter were calculated at the surface, N_0 and λ_0.

The first parameter, N_0, was estimated from the vapor pressure of the sublimated molecule through the expression:

$$N_0 = \frac{P_v(T)}{m \cdot g_0} \tag{14}$$

in which g_0 is the gravitational intensity $\frac{G \cdot M_0}{r_0^2}$ and m and P_v represent the mass and vapor saturation pressure of the corresponding volatile. The Jeans escape parameter was obtained using

$$\lambda_0 = \frac{M \cdot m \cdot G}{k \cdot T \cdot r_0} \tag{15}$$

where M and m are the masses of the body and molecule (N_2 in this case), respectively (kg); G is the gravitational constant; k is the Boltzmann constant; T is the absolute body temperature at the surface; and r_0 is the radius.

This new curve that was obtained and inserted in Figure 7 is remarkably slowed to the left, meaning that all of the objects that are located on or to the left of the original N_2 line, and that are obtained considering only the Jeans escape mechanism, are now clearly to the right except for 474640 Alicanto (2004 VN112).

As previously indicated, the regime acquired for the molecules' escape is directly related to the surface molecular density, therefore meaning that it is directly related to the vapor pressure. It is important to take into account the temperature variations of these bodies in their journey around the Sun, considering the possibility that the loss of volatiles has been over- or underestimated. This is the reason why this study has also updated Figure 1 from Johnson et al. (2015) for a rich nitrogen atmosphere.

To perform this analysis, the column density and the Jeans escape parameter at the surface, N_0 and λ_0, were estimated from Equations (14) and (15).

The results obtained are represented in Figure 8, where λ_0 is plotted versus N_0 for several objects along their corresponding evolution as they move through their orbit around the Sun.

The solid line in Figure 8 represents the points where the N_2 loss, in the case in which this molecule will be found in the original inventory of ices on each body, estimated by the Jeans escape mechanism matches with that predicted by Johnson et al. (2015), taking into account the hydrodynamic escape mechanism in the latter. This curve was obtained by setting R_{fit} in Equation (13) equal to 1. According to the position with respect to this curve, it is possible to observe two different behaviors, one of them representing objects as Eris, Triton, Pluto, Makemake, or Sedna (except at its aphelion) lying above this line, and therefore demonstrating that the corresponding escaping rate has been underestimated, and in the other, representing the objects as Quaoar, Orcus, Varuna, and Gonggong (except at its perihelion), and therefore demonstrating that this parameter has been overestimated. These results can be applied to accurate the lines obtained in Figure 7

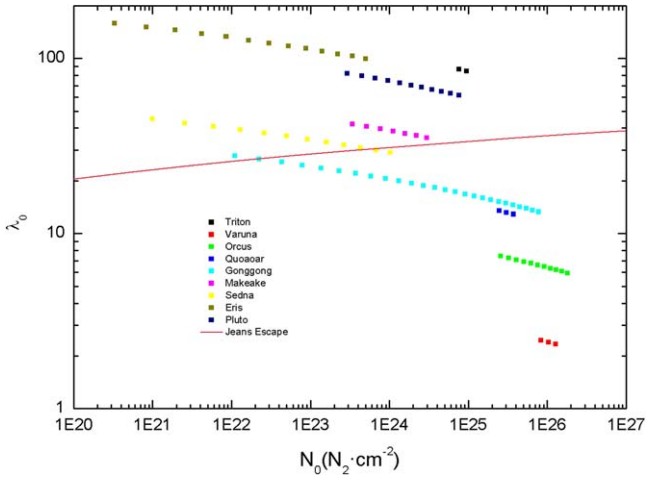

Figure 8. The Jeans escape parameter is plotted vs. column density for an atmosphere dominated predominantly by N_2 molecules, which is the most volatile one, both obtained from our vapor pressure values. The evolution of the curves for each object represents the change in temperature for this object in its path around the Sun. The temperature data have been obtained from Prialnik et al. (2020).

because in Figure 8 the actual temperature range has not been substituted by an equilibrium temperature. It is clear that if the trajectory for a particular body is above or below this solid line, the conclusions indicated in this paragraph will be applied; however, if the trajectory crosses the solid line, it is possible that the overestimated and underestimated loss will be compensated, depending on its trajectory around the Sun.

The most remarkable point is that by considering the measurements of N_2 vapor pressure obtained in this study, in all cases N_0 corresponds to values that are well above 10^{20}. It is important to consider this fact, especially given that this would imply a higher CH_4 amount than previously assumed, and therefore meaning that the effect of global warming would be higher than previously considered. Johnson et al. (2015) exposed that if the N_2 columnar density was equal to or greater than 10^{18} $N_2 \cdot cm^{-2}$, and assuming a CH_4 relative concentration to N_2 of 2% or 3%, the atmosphere would be thick enough for Lyman-α radiation to interact with methane and contribute to atmospheric warming.

The columnar densities obtained from the pressure-measured values in the laboratory used in this study far exceed this value, clearly proving that the conclusions expressed in previous works should be reconsidered.

7. Conclusions

The presence of the solid and gas phases of molecules in many astrophysical scenarios led to the decision to study the parameters that determine the dynamics in these systems. Vapor pressure is considered a necessary parameter in order to undertake this study. In this study, this quantity was determined using a QCMB, the main feature of which is its ability to directly detect the molecules releasing from its surface.

The sublimation rates for the molecules involved in this study were experimentally determined at several constant temperatures. These values were used to determine the vapor pressures according to the mathematical procedure explained above. The results obtained for H_2O, CO_2, and CH_3OH ice were used to check the validity of the procedure presented based on previous reviews on this molecule in the literature.

As a result, the vapor pressures for eight different molecules of astrophysical interest have been reported at temperatures related to scenarios of interest in this area. The values obtained in the present work for the molecules C_2H_6 and C_2H_4 are the first to be reported in the literature for the range of temperatures used in this study without using mathematical extrapolations. N_2, CO, and CH_4, together with the values that appear in the work of Grundy et al. (2024), constitute the first values obtained in the temperature range with interest in the studies focusing on KBOs and TNOs.

Concerning the presence of ices in KBOs and TNOs, the contribution that the hydrodynamic flow could cause on N_2 was also considered. This already appears in previous works; however, the results attained were surprising given that the vapor pressure values that were obtained for the N_2 molecule were higher than those recorded in previous databases. This is relevant because different studies highlight the influence that atmospheric heating, produced by the interaction of ultraviolet radiation with CH_4 molecules, can produce on the volatiles' escape. This effect starts to become quantitatively important for values around 10^{18} molecules cm^{-2} for N_2, considering a relative richness of between 2% and 3% of CH_4 with respect to N_2. However, with the values presented in this study, the columnar densities obtained were up to several orders of magnitude higher than those predicted by previous works, which should lead to a significant change in the relative weight of the role played by each escape mechanism.

Acknowledgments

This research has been funded with the project PID2020-118974GB-C22 by the Spanish Ministry of Science and Innovation.

ORCID iDs

C. Millán https://orcid.org/0000-0002-8373-5808
R. Luna https://orcid.org/0000-0001-8792-7578
M. Domingo https://orcid.org/0000-0002-7527-3797
C. Santonja https://orcid.org/0000-0002-1015-8982
M. Á. Satorre https://orcid.org/0000-0002-4787-5694

References

Barucci, M. A., Cruikshank, D.P., Dotto, E., et al. 2005, A&A, 439, L1
Barucci, M. A., Dalle Ore, C.M., Perna, D., et al. 2015, A&A, 584, A107
Benes, E. 1984, JAP, 56, 608
Borovik, E. S., Grishin, S. F., & Grishina, E. Y. 1960, SPTP, 5, 506
Brown, M. E., Burgasser, A. J., & Fraser, W. C. 2011, ApJ, 738, L26
Bryson, C. E., Cazcarra, V., & Levenson, L. L. 1974, J. Chem. Eng. Data, 9, 107
Colling, M. P., Mark, M.A., & Chen, R. 2004, MNRAS, 354, 1133
Cook, C. J., Dalle Ore, C.M., Protopapa, S., et al. 2019, Icar, 331, 148
Coustenis, A., Achterberg, R.K., Conrath, B.J., et al. 2007, Icar, 189, 35
Cruikshank, D. P., Roush, T.L., Owen, T.C., et al. 1993, Sci, 261, 742
Dalle Ore, C. M., Barucci, M.A., Emery, J.P., et al. 2015, Icar, 252, 311
Dalton, J. B., Cruikshank, D. P., Stephan, K., et al. 2010, SSRv, 153, 113
Emery, J. P., Wong, I., Brunetto, R., et al. 2024, Icar, 414, 116017
Fray, N., & Schmitt, B. 2009, P&SS, 57, 2053
González Díaz, C, Carrascosa, H, Muñoz Caro, G M, Satorre, M Á, & Chen, Y-J 2022, MNRAS, 517, 5744
Grundy, W.M., Binzel, R.P., Buratti, B.J., et al. 2016, Sci, 351, 9189G
Grundy, W.M., Tegler, S.C., Steckloff, J.K., et al. 2024, Icar, 410, 115767
Hudson, R. L., Gerakines, P. A., & Moore, M. H. 2014, Icar, 243, 148
Johnson, R. E., Oza, A., Young, L. A., Volkov, A. N., & Schmidt, C. 2015, ApJ, 809, 43
Johnson, R. E., Volkov, A. N., & Erwin, J. T. 2013a, ApJ, 779, L30
Johnson, R. E., Volkov, A. N., & Erwin, J. T. 2013b, ApJL, 768, L4

Langmuir, I. 1913, PhRv, 2, 329
Licandro, J., Pinilla-Alonso, N., Pedani, M., et al. 2006, A&A, 445, L35
Lisse, C. M., Young, L.A., Cruikshank, D.P., et al. 2021, Icar, 356, 114072
Lodders, K., & Fegley, B., Jr 1998, The Planetary Scientist's Companion (Oxford: Oxford Univ. Press)
Lucas, S., Ferry, D., Demirdjian, B., & Suzanne, J. 2005, JPCB, 109, 18103
Luna, R., Domingo, M., Millán, C., Santonja, C., & Satorre, M.Á. 2018, Vacuu, 152, 278
Luna, R., Millán, C., Domingo, M., & Satorre, M. Á. 2008, Ap&SS, 314, 113
Luna, R., Millán, C., Domingo, M., Santonja, C., & Satorre, M. A. 2012, Vacuu, 86, 1969
Luna, R., Millán, C., Domingo, C., Santonja, M. A., & Satorre, M. Á. 2022, ApJ, 935, 134
Mauersberger, K., & Krankowsky, D. 2003, GeoRL, 30, 1121
McCord, T. B., Hayne, P., Combe, JP, et al. 2008, Icarus, 194, 212
Muñoz Caro, G. M., Jiménez-Escobar, A., Martín-Gago, J. Á., et al. 2010, A&A, 522, A108
Murphy, D. M., & Koop, T. 2005, QJRMS, 131, 1539
Owen, T. C., Roush, T.L., Cruikshank, D.P., et al. 1993, Sci, 261, 745
Perna, D., Hromakina, T., Merlin, F., et al. 2017, MNRAS, 466, 3594
Prialnik, D., Barucci, M. A., & Young, L. 2020, in The Trans-Neptunian Solar System., ed. D. Prialnik, M. A. Barucci, & L. A. Young (Amsterdam: Elsevier), 12
Satorre, M. Á., Millán, C., Molpeceres, G., et al. 2017, Icar, 296, 179
Satorre, M. Á., Luna, R., Millán, C., Domingo, M., & Santonja, M. C. 2018, Ap&SS, 451, 51
Sauerbrey, G. Z. 1957, Phys. Verhandl, 8, 193
Sauerbrey, G. Z. 1959, PhyZ, 155, 206
Schaller, E. L., & Brown, M. E. 2007, ApJ, 659, L61
Schulze, W., & Abe, H. 1980, CP, 52, 381
Tegler, S. C., Cornelison, D.M., Grundy, W.M., et al. 2010, ApJ, 725, 1296
Volkov, A. N., Johnson, R. E., Tucker, O. J., & Erwin, J. T. 2011a, ApJ, 729, L24
Volkov, A. N., Tucker, O. J., Erwin, J. T., & Johnson, R. E. 2011b, PhFl, 23, 066601
White, B. E., Hessinger, J., & Pohl, R. O. 1998, JLTP, 111, 233